PAPER

Check for updates

Concentration-dependent spectroscopic properties and temperature sensing of YNbO₄:Er³⁺ phosphors

Xin Wang,[a] Xiangping Li, [ID] *[a] Lihong Cheng,[a] Sai Xu,[a] Jiashi Sun,[a] Jinsu Zhang,[a] Xizhen Zhang,[a] Xiaotian Yang[b] and Baojiu Chen*[a]

A series of YNbO₄:Er³⁺ phosphors with various Er³⁺ concentrations was synthesized *via* a traditional high temperature, solid-state reaction method. XRD Rietveld refinements based on the XRD data were carried out to study the phase purity and crystal structure of the as-prepared samples. The results revealed that single monoclinic phase YNbO₄ phosphors were obtained. The influence of the Er³⁺ concentration on the spectroscopic properties and temperature sensing in YNbO₄:Er³⁺ phosphors were systematically studied. Different quenching concentrations were found in down-conversion and up-conversion luminescence processes. From lasers working current dependent up-conversion luminescence spectra, it was confirmed that two and three photon processes were responsible for both the green and the red up-conversion emissions, respectively, excited by 980 and 1550 nm lasers, which have no apparent dependence on Er³⁺ ion concentration. However, the Er³⁺ concentration had significant influences on the temperature sensing sensitivity of Er³⁺ ions, and the results showed that YNbO₄ phosphors doped with low concentrations of Er³⁺ ions had high temperature sensing sensitivity and could be applied in temperature detection applications, particularly in high temperature environments.

1. Introduction

In recent years, rare earth (RE) ion-doped, luminescent materials have received great interest due to their potential applications in several fields, such as display devices, solid-state lasers, sensors, and optoelectronic devices.[1–4] The application of RE ion-doped luminescent materials, as optical temperature sensors, has become increasingly popular due to the fact that their non-contact temperature measurement is carried out by probing the temperature dependence of the fluorescence intensities ratio (FIR) from the two thermally coupled emitting energy levels. Real-time temperature detection can be achieved by analyzing the changes in the FIR values caused by the change in sample temperature.[5] Compared with traditional temperature monitoring devices, the FIR technique for temperature measurement can effectively reduce the influence of measuring conditions and improve the temperature resolution.[6–8] In order to obtain high temperature sensitivity using RE³⁺ as the temperature sensing units, the energy separation between the two emitting energy levels of RE³⁺ must be moderate. It should neither be too small (<200 cm⁻¹) to avoid strong overlap of the two emissions nor too large (>2000 cm⁻¹) to ensure the upper

level possess enough population of optically active ions in a certain temperature range.[9] Among a large number of RE³⁺ ions, Er³⁺ is expected to be an effective temperature sensing unit with high sensing sensitivity due to its two thermally coupled emitting energy levels ²H₁₁/₂ and ⁴S₃/₂, which have a proper energy gap of around 770 cm⁻¹ and can obtain two significant green emissions.[10]

Usually, fluorides are promising host materials for up-conversion (UC) luminescence due to their low phonon energy, which is beneficial to high UC luminescence efficiency. However, compared with fluorides, oxide matrix materials are much more suitable to be used in high temperature environments due to their good chemical and physical stabilities and have received extensive attention in recent years.[11] Among various oxide matrixes, ANbO₄ (A = La, Gd, Y) compounds with a fergusonite structure are good choices as the matrixes of UC luminescent phosphors due to their lower phonon frequencies than other oxide compounds.[12–14] Recently, some investigations on the UC luminescence and temperature sensing properties of Er³⁺ in ANbO₄ have been reported. B. N. Tian *et al.* pointed out that the UC luminescence intensity and temperature sensing sensitivity can be enhanced by introducing Mo⁶⁺ into a LuNbO₄:Er³⁺ phosphor.[15] Y. Y. Tian *et al.* reported that the Yb³⁺ concentration has a significant influence on the UC luminescence and temperature sensing behavior of Er³⁺ in Yb³⁺/Er³⁺ co-doped YNbO₄.[14] Singh *et al.* reported a dual mode Y₀.₉₇₇Yb₀.₀₂Er₀.₀₀₃NbO₄ phosphor demonstrating both down-conversion (DC) and UC emission, and this type of phosphor could

[a]*Department of Physics, Dalian Maritime University, Dalian, Liaoning, 116026, PR China. E-mail: lixp@dlmu.edu.cn; chenmbj@sohu.com*

[b]*Jilin Provincial Key Laboratory of Architectural Electricity & Comprehensive Energy Saving, Jilin Jianzhu University, Changchun 130118, China*

be an exceptional choice for next generation, luminescence-based, temperature sensing devices.[16] However, Er^{3+} acts as a temperature sensing unit, and its doping concentration may have significant influences on the spectroscopic and temperature sensing properties in $ANbO_4$. Therefore, it is necessary to conduct a study on the influence of Er^{3+} concentration on the spectroscopic and temperature sensing behavior of Er^{3+} in $ANbO_4$ phosphors.

In this study, $YNbO_4:Er^{3+}$ phosphors with various Er^{3+} concentrations were prepared by a traditional high temperature solid-state reaction method. Er^{3+} concentration-dependent DC, UC luminescence and temperature sensing properties were systematically studied.

2. Experimental

A series of $Y_{1-x}Er_xNbO_4$ phosphors ($x = 0.5, 1, 3, 5, 7, 9, 12, 15, 20, 30, 40, 60$ and 80%, in molar) were synthesized via a traditional high temperature solid-state reaction method. First, the starting materials including Y_2O_3 (99.99%), Nb_2O_5 (99.99%) and Er_2O_3 (99.99%) were weighed according to a certain stoichiometric ratio, and then they were uniformly mixed in an agate mortar. Furthermore, the mixture was delivered into a crucible, it was put into a muffle furnace and calcined at 1300 °C for 4 h.

Last, the final products were obtained after the furnace naturally cooled to room temperature.[17]

The crystal structures of the samples were analyzed on a Shimadzu XRD-6000 diffractometer (Japan) equipped with Cu $K\alpha_1$ as the radiation source ($\lambda = 0.15406$ nm). Both UC and DC luminescence spectra were measured using a Hitachi F-4600 spectrophotometer. The former measurements were achieved using two externally introduced lasers with wavelengths of 980 and 1550 nm, but the latter one was performed with the spectrophotometer built-in excitation source (150 W xenon lamp). The sample temperatures were controlled by a self-manufactured temperature control system, DMU TC-450, with a controlling accuracy of about ±0.5 °C.

3. Results and discussion

In order to identify the crystal structure of the final products, XRD measurements were performed on all the samples, and all of them almost had the same diffraction patterns. Fig. 1 shows the XRD patterns of x mol% Er^{3+}-doped $YNbO_4$ ($x = 15, 40, 60$ and 80) as representatives. In order to better study the effect of Er^{3+} doping on the crystal structure of $YNbO_4$, a Rietveld refinement procedure was carried out with a non-commercial
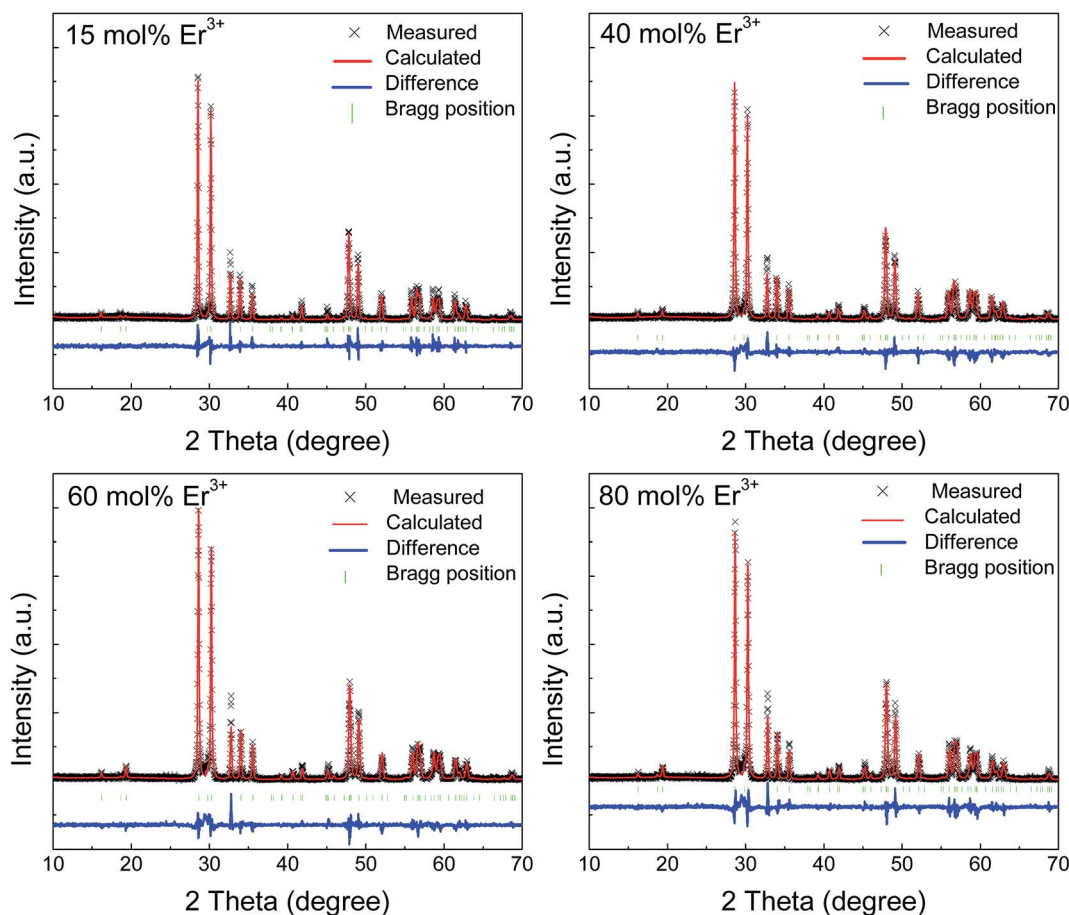

Fig. 1   XRD patterns of $YNbO_4:x$ mol% Er^{3+} ($x = 15, 40, 60$ and 80) phosphors. Multiplication signs represent the experimental data, the red curves accompanying the asterisks show the Rietveld refinement results, the green sticks mark the Bragg reflection positions, and the blue solid lines represent the differences between experimental and calculated data.

Table 1 Rietveld refinement results and crystal data for $YNbO_4$:x mol% Er^{3+} (x = 15, 40, 60 and 80) phosphors

Formula	$Y_{0.85}Er_{0.15}NbO_4$	$Y_{0.6}Er_{0.4}NbO_4$	$Y_{0.4}Er_{0.6}NbO_4$	$Y_{0.2}Er_{0.8}NbO_4$
Radiation type	Cu Kα_1 radiation with $\lambda = 1.5406$ Å			
2θ range	10–70°			
Symmetry	Monoclinic system			
Space group	$C2/c$ (15)			
Cell parameters	$a = 7.608$ Å	$a = 7.602$ Å	$a = 7.598$ Å	$a = 7.588$ Å
	$b = 10.934$ Å	$b = 10.922$ Å	$b = 10.916$ Å	$b = 10.905$ Å
	$c = 5.291$ Å	$c = 5.285$ Å	$c = 5.281$ Å	$c = 5.275$ Å
	$\alpha = \gamma = 90°$	$\alpha = \gamma = 90°$	$\alpha = \gamma = 90°$	$\alpha = \gamma = 90°$
	$\beta = 138.416°$	$\beta = 138.389°$	$\beta = 138.370°$	$\beta = 138.357°$
	$V = 292.131$ Å^3	$V = 291.430$ Å^3	$V = 290.958$ Å^3	$V = 290.057$ Å^3
Reliability factors	$\chi^2 = 1.744$	$\chi^2 = 2.196$	$\chi^2 = 2.003$	$\chi^2 = 2.304$
	$R_{wp} = 21.69\%$	$R_{wp} = 22.69\%$,	$R_{wp} = 21.07\%$	$R_{wp} = 22.27\%$
	$R_p = 15.37\%$	$R_p = 15.99\%$	$R_p = 14.31\%$	$R_p = 15.62\%$

software, GSAS.[18,19] In the fitting process, the crystallographic data of monoclinic $YNbO_4$ (space group of $C2/c$ (15), see JPCDS card no. 83-1319) were used as the initial crystal structure model. The measured, calculated results, Bragg position, and the difference between experimental and theoretical diffraction patterns are also shown in Fig. 1. It can be seen that all the diffraction peaks in the experimental data can be fitted well by the Rietveld theoretical model, and the differences between experimental and theoretical data seem to be acceptable. The cell parameters and the Rietveld refinement results are shown in Table 1, which demonstrate that all the observed diffraction peaks satisfy the reflection conditions, and our as-prepared samples are of single monoclinic phase.

Fig. 2 shows the excitation spectra of $YNbO_4$ samples doped with various Er^{3+} concentrations monitored at a 555 nm emission corresponding to the $^4S_{3/2} \rightarrow {}^4I_{15/2}$ transition of Er^{3+}. As can be seen, each spectrum comprises of two parts. One is a broad band ranging from 200 to 300 nm corresponding to the absorption of NbO_4^{4-}.[20] Another part is composed of some narrow peaks belonging to the characteristic f–f transitions of Er^{3+} from the ground state $^4I_{15/2}$ level to the excited state levels $^4G_{11/2}$, $^2H_{9/2}$, $^4F_{3/2}$, $^4F_{5/2}$, $^4F_{7/2}$ and $^2H_{11/2}$, respectively. It is
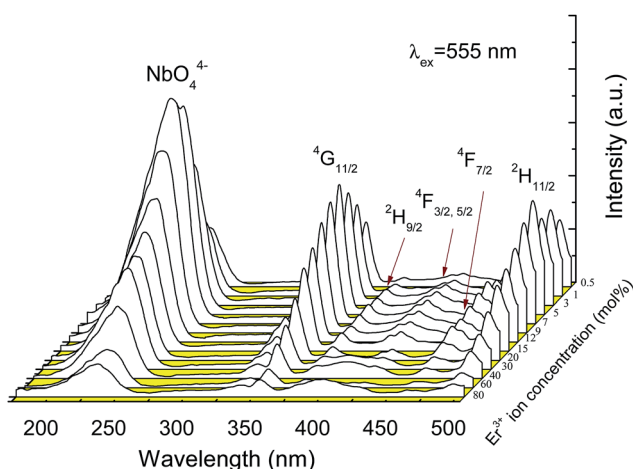
noteworthy that the excitation intensity of NbO_4^{4-} is a little stronger than that of the strongest f–f transition of Er^{3+}, indicating that there is an effective energy transfer from the host matrix to Er^{3+}.

Fig. 3 shows the emission spectra of $YNbO_4$ samples doped with various Er^{3+} concentrations measured under 379, 980 and 1550 nm excitations. From Fig. 3(a), it can be found that two green emissions, which originate from the characteristic transitions ($^2H_{11/2}$, $^4S_{3/2}$) $\rightarrow {}^4I_{15/2}$ of Er^{3+}, dominate the whole DC spectra, together with a weak red emission centered at around 657 nm corresponding to the $^4F_{9/2} \rightarrow {}^4I_{15/2}$ transition of Er^{3+}.[10] Moreover, it can also be found that with an increase in the Er^{3+} concentration, the green emission intensities first increase and reach their maximum values at around 5 mol% of Er^{3+}, and then decline with further increases in Er^{3+} concentration, indicating the occurrence of concentration-based quenching.[21]

As can be seen from the UC luminescence spectra excited by 980 and 1550 nm lasers (Fig. 3(b) and (c)), strong green and red UC emissions were both observed. Moreover, the intensities of the green and the red emissions first dramatically increased as the concentration of Er^{3+} increased, and the intensities decreased when the Er^{3+} concentration was greater than 40 mol%, implying the occurrence of concentration-based quenching in the UC luminescence processes. At higher doping concentrations of Er^{3+}, the interaction between Er^{3+} was enhanced due to a decrease in the interionic distance, which induced an increase in the non radiative relaxation rate, which resulted in the quenching of luminescence under both DC and UC luminescence processes.

The quenching concentration is usually defined as a concentration at which the maximum luminescence intensity can be achieved. It should be noted that the quenching concentrations for the DC and UC luminescence processes were greatly different, which can be ascribed to the different excitation pathways and population routes.[22] For the concentration quenching process of DC luminescence, Van Uitert developed a model to describe the relationship between the luminescent intensity and the doping concentration of the luminescent center, which can be expressed as follows:[23]

$$I(C) = C/k[1 + \beta C^{Q/3}] \tag{1}$$

Fig. 2 Excitation spectra of $YNbO_4$ samples doped with various Er^{3+} concentrations by monitoring the 555 nm emission.

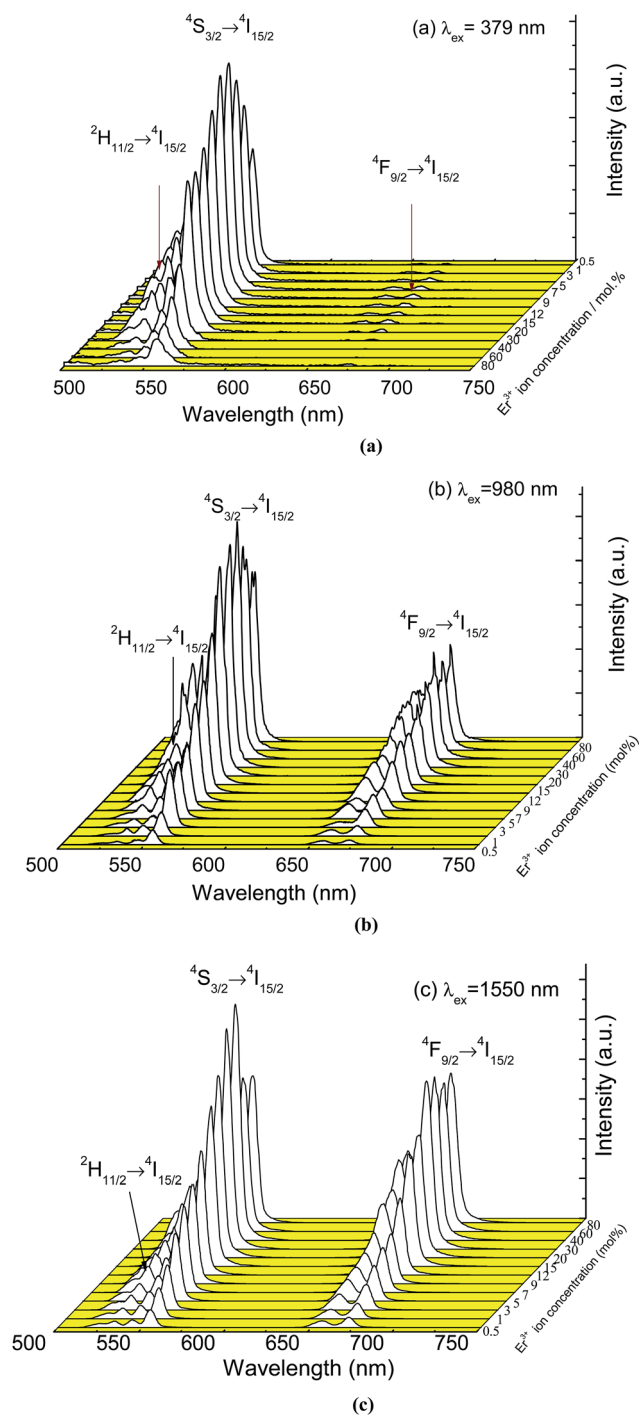**Fig. 3** Emission spectra of YNbO$_4$ samples doped with various Er^{3+} concentrations excited at 379 nm (a) and 980 nm (b) and 1550 nm (c).

was used to fit the experimental data displayed in Fig. 4(a) for the integrated intensities of the green DC emissions. The red solid curve shows the results of curve fitting. It can be seen that the experimental data are in agreement with the Van model. In the fitting process, the Q value was derived to be 5.64, which undoubtedly implies that the energy transfer behavior between Er^{3+} in YNbO$_4$:Er^{3+} phosphors was dominated by the electric dipole–dipole interaction. As mentioned above, concentration quenching also existed in the UC luminescence process. However, there is no mature theory to describe the quenching behavior. The solid curves in Fig. 4(a) only show the change in trend of the integrated green UC luminescence intensities towards the Er^{3+} concentration in both the cases of 980 and 1550 nm excitation.

Comparing the three sets of luminescence spectra shown in Fig. 3, it can also be found that the relative intensity of the green and the red emissions are significantly different. For the DC luminescence process, when pumped by 379 nm, the electrons first populate the higher energy level $^4G_{11/2}$ of Er^{3+} and then nonradiatively relax to the lower $^2H_{11/2}$ and $^4S_{3/2}$ levels, from which the electrons further radiative transit to the ground state $^4I_{15/2}$ level and achieve green emissions, which can be seen in Fig. 5. In addition, some electrons at $^2H_{11/2}$ and $^4S_{3/2}$ levels may further relax to the $^4F_{9/2}$ level and exhibit a red emission. However, these emission levels can be populated by phonon-assisted, multi-photon absorption in the UC luminescence processes excited by both 980 and 1550 nm infrared wavelengths. Particularly, the population of the $^4F_{9/2}$ level can be achieved much more effectively than that of the excitation at 379 nm. Consequently, much stronger red emissions were obtained under both 980 and 1550 nm excitations than under 379 nm excitation.

In order to further explore the UC luminescent mechanism, laser working current dependent UC luminescence spectra were measured. Fig. 6(a) and (b) display the integrated green and red UC luminescence intensities of the as-prepared YNbO$_4$:x mol%
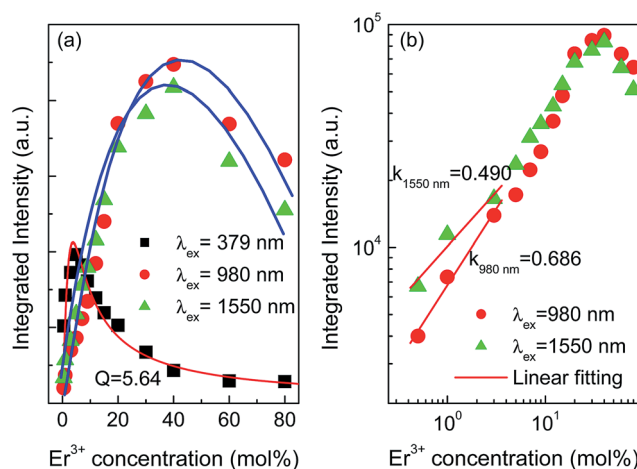
where $I(C)$ is the integrated intensity of DC luminescence, C is the luminescent center concentration, k and β are constants, which depend upon the host matrixes and specific RE^{3+}, and Q represents the interaction mechanism between RE^{3+}. Q is equal to 3, 6, 8 or 10, which represents exchange, electric dipole–dipole, dipole–quadrupole and quadrupole–quadrupole interactions, respectively. For the sake of recognizing the concentration quenching process of YNbO$_4$:Er^{3+} phosphors, eqn (1)

Fig. 4 (a) Dependence of the integrated emission intensities of $^2H_{11/2}$, $^4S_{3/2} \rightarrow \ ^4I_{15/2}$ transitions on Er^{3+} concentrations excited at 379, 980 and 1550 nm. (b) Er^{3+} concentration-dependent UC luminescence intensity in a double logarithm coordinate system.
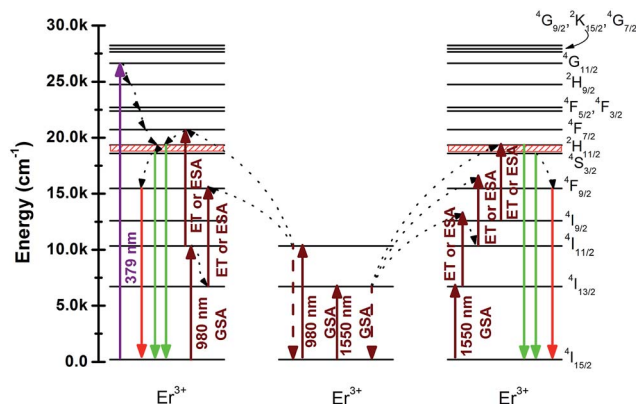
Fig. 5 Energy level diagrams of Er^{3+} and the possible DC and UC luminescence mechanisms of $YNbO_4:Er^{3+}$ samples under 379 nm and 980, 1550 nm excitations.

Er^{3+} ($x = 5, 15, 40$) phosphors at different laser working currents under 980 and 1550 nm excitations. As is well-known, the number of the photons (n), which take part in the multi-photon
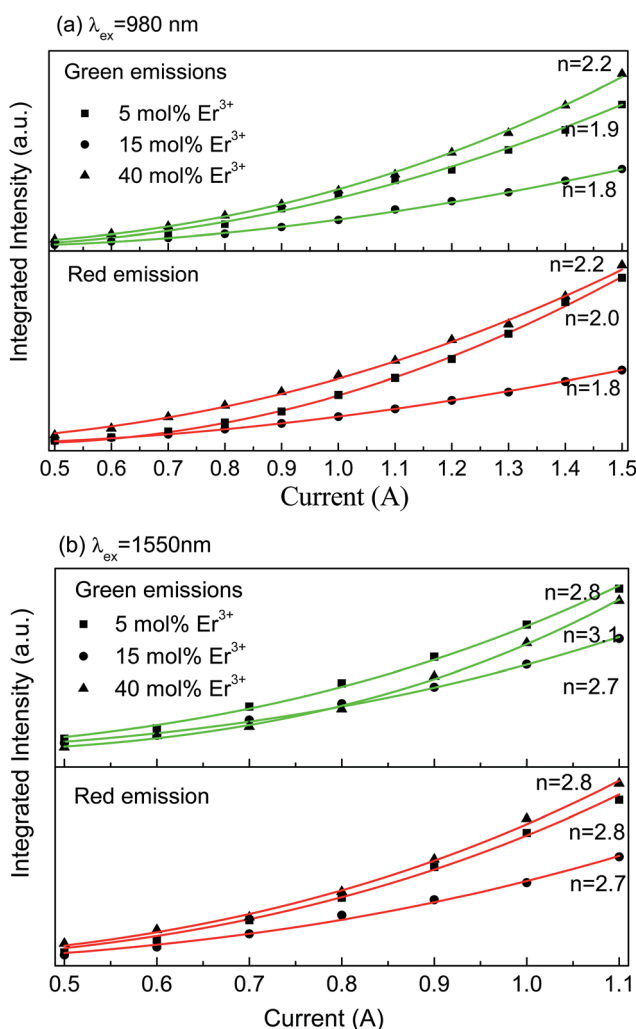

Fig. 6 The relationship between the integrated UC luminescence intensities and laser working current under 980 nm (a) and 1550 nm (b) laser excitations.

absorption UC luminescence processes, can be determined from the dependence of the luminescence intensity (I_{up}) on the laser working current (i_{LD}), which fulfills $I_{up} \propto (ai_{LD} - b)^n$, where a and b are exponential constants.[24] The integrated green and red UC emission intensities were fitted to this relation, and the n values for the two UC emissions derived from the fitting processes are shown in Fig. 6. It can be seen that whether the Er^{3+} concentration is high or low, n values of 2 were obtained at an excitation of 980 nm for both the green and the red UC emissions, and 3 photons were needed for both the green and the red UC emissions under 1550 nm excitation. The little differences for those values may be caused due to the calculated error of the integrated intensity and from the fitting process. This means that two-photon and three-photon processes were respectively dominated in the UC luminescent processes when excited at 980 and 1550 nm in $YNbO_4:Er^{3+}$ phosphors. Moreover, the Er^{3+} doping concentration had no significant influence on the UC luminescence processes for both 980 nm and 1550 nm excitations. The different number of photons under 980 and 1550 nm excitations can be ascribed to the different UC luminescence mechanisms. The possible mechanisms for the UC emissions in $YNbO_4:Er^{3+}$ samples excited at 980 nm and 1550 nm are shown in the schematic energy level diagrams of Er^{3+} ions (Fig. 5).

It should be noted that the green and red UC emissions mainly originated from both the energy transfer (ET) between Er^{3+} and the excited state absorption (ESA) of Er^{3+}. Under an excitation of 980 nm, Er^{3+} was first excited from the ground state $^4I_{15/2}$ level to the $^4I_{11/2}$ level by absorbing one 980 nm photon, namely GSA: $^4I_{15/2}$ + a photon → $^4I_{11/2}$. Then, this Er^{3+} may transfer its energy to another Er^{3+} (ET process) in the $^4I_{11/2}$ level or absorb another 980 nm photon (ESA process), thus resulting in the population of $^4F_{7/2}$ level of Er^{3+}. Then, the Er^{3+} in $^4F_{7/2}$ level non radiatively relaxes to the $^2H_{11/2}$ levels ($^4F_{7/2}$ → $^2H_{11/2}$ + phonons). Finally the green emissions from $^2H_{11/2}$ and $^4S_{3/2}$ levels can be achieved (($^2H_{11/2}$, $^4S_{3/2}$) → $^4I_{15/2}$ + photon) because $^2H_{11/2}$ and $^4S_{3/2}$ levels exist in thermal equilibrium. In addition, the excited Er^{3+} in $^4I_{11/2}$ level can also non radiatively relaxes to the $^4I_{13/2}$ level via a multi-phonon relaxation process due to the small distance in energy between these two energy levels. The Er^{3+} in the $^4I_{13/2}$ level can accept the energy from another Er^{3+} in $^4I_{11/2}$ via an ET process or an ESA process to get into $^4F_{9/2}$ level, and then the red emission can be achieved through a $^4F_{9/2}$ → $^4I_{15/2}$ transition.[25] These population and radiation processes are depicted on the left hand side of Fig. 5.

For the 1550 nm excitation, both the green and the red UC emissions must absorb three 1550 nm photons. The population processes are clearly shown on the right hand side of Fig. 5. When excited at 1550 nm, the Er^{3+} in the ground state $^4I_{15/2}$ level is first excited to the $^4I_{13/2}$ level via a GSA process, and the $^2H_{11/2}$ and $^4S_{3/2}$ levels can be populated via an ET or ESA processes (right hand side of Fig. 5), thus yielding the green emissions.[26] The population of the $^4F_{9/2}$ level strongly influences the red UC emission. The possible population approach is that the Er^{3+} in the $^4I_{9/2}$ level nonradiatively relaxes to the $^4I_{11/2}$ level, and then goes to the $^4F_{9/2}$ level via an ET or an ESA process. Therefore, the

red UC emission could be achieved when Er^{3+} radiatively transits to the ground state $^4I_{15/2}$ level.

It is needless to say that the interaction between Er^{3+} in Er^{3+} mono-doped samples is weak when the Er^{3+} doping concentration is low. Therefore, the ESA process is probably the main mechanism for UC emissions of Er^{3+}. In this case, UC luminescent intensity would be proportional to the doping concentration of Er^{3+}. To clarify the UC mechanism for our samples doped with low Er^{3+} concentrations, Er^{3+} concentration-dependent, UC intensity is plotted in a double logarithm coordinates system as shown in Fig. 4(b), and the data obtained under 980 and 1550 nm excitations in the low Er^{3+} concentration region are fitted to a linear function. The slopes from the fitting processes were lower than 1 (0.686 for 980 nm excitation and 0.490 for 1550 nm excitation), implying that there was not only one Er^{3+} involved in the UC luminescence process, but two or more Er^{3+} contributed to the UC emissions in both 980 and 1550 nm excitations. That is to say, there are obvious interactions (ETs) between Er^{3+}, but not only the ESA process is in charge of the UC luminescence even at low Er^{3+} doping concentrations.

Usually, the temperature has a big influence on the spectroscopic properties of both DC and UC luminescent materials. Moreover, the thermal stability of the spectroscopic properties of phosphors is extremely essential to assess the performance of the luminescent materials since the materials may be used in a high temperature environment. Temperature-dependent, DC luminescence properties of $YNbO_4$:Er^{3+} phosphors were systematically investigated in this study. Fig. 7 shows the temperature dependence of DC emission spectra of $YNbO_4$:x mol% Er^{3+} ($x = 3, 9, 15, 30$) samples as representatives, which were measured in the temperature region ranging from 20 °C to 450 °C. As shown in Fig. 7, two sets of clear green emissions originating from $(^2H_{11/2}, ^4S_{3/2}) \rightarrow {}^4I_{15/2}$ of Er^{3+} were observed,

and with an increase in sample temperature, their peak positions remained almost the same, but their relative intensities and changing trends were quite different from each other. It can be seen that in the two sets of emission spectra, the intensities of the green emission originated from the $^4S_{3/2} \rightarrow {}^4I_{15/2}$ transition both decreased monotonically with an increase in temperature, clearly implying a thermal quenching behavior. In contrast, the intensities of the green emission first came from the $^2H_{11/2} \rightarrow {}^4I_{15/2}$ transition and slightly increased, then remain almost unchanged. The different trends in variation for these two green emissions indicated an increase in the thermal population rate from the $^4S_{3/2}$ level to $^2H_{11/2}$ level at higher temperatures. However, the intensity ratio of the two green emissions had different trends with any green emission. Fig. 8 shows the dependences of the FIR values (R, I_H/I_S) of these two green emissions on temperature for $YNbO_4$:x mol% Er^{3+} ($x = 3$, 9, 15, 30) phosphors, where I_H and I_S are the fluorescence intensities from $^2H_{11/2} \rightarrow {}^4I_{15/2}$ and $^4S_{3/2} \rightarrow {}^4I_{15/2}$ transitions, respectively. It can be clearly seen that the ratio of these two green emissions monotonically increased with an increase in temperature.

The energy distance between $^2H_{11/2}$ and $^4S_{3/2}$ levels was small, and they existed in a state of thermal equilibrium; thus their populations followed the Boltzmann distribution.[25] The value of R for the two green emissions was a temperature dependent variable, and the relationship between them can be expressed as follows:

$$R(T) = I_H/I_S = A\exp(-\Delta E/kT) \qquad (2)$$

where ΔE is the energy distance between $^2H_{11/2}$ and $^4S_{3/2}$ levels, k is Boltzmann's constant, and T is the absolute temperature.[27] From eqn (2), it can be seen that the R value is only related to the sample temperature T for a specific sample; thus the sample
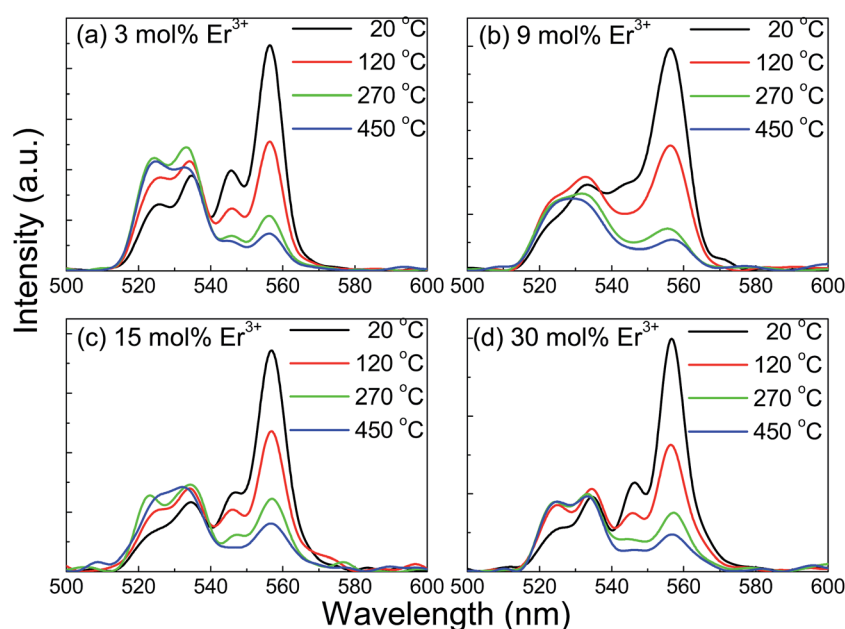

Fig. 7 Temperature dependent DC emission spectra for $YNbO_4$:x mol%Er^{3+} ($x = 3, 9, 15, 30$) under 379 nm excitation.
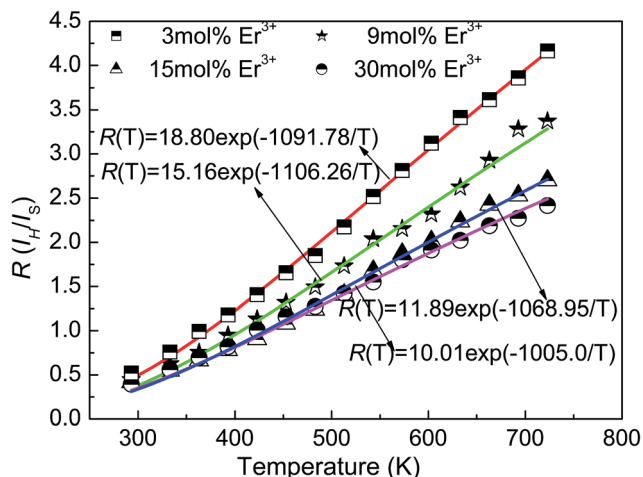
Fig. 8 Dependences of the FIR values (R, I_H/I_S) of the two green emissions on temperature for YNbO$_4$:x mol% Er^{3+} (x = 3, 9, 15, 30) phosphors.

Table 2 Values of sensitivity of Er^{3+} in different host materials

Host material	Maximum sensitivity (10^{-4} K^{-1})	Temperature (K)	Ref.
YNbO$_4$ phosphors	93	554	This work
YNbO$_4$ nanoparticles	72	406	14
YNbO$_4$ phosphors	73	472	16
Chalcogenide glass	102	493	27
ZnO-nanocrystals	62	443	28
Fluorindate glass	54	547	29
Silicate glass	23	296	30
PLZT glass-ceramic	19	556	31
Fluorozirconate glass	6	300	32

temperature can be achieved by measuring the R value. To understand the temperature sensing properties of YNbO$_4$:Er^{3+} phosphors, eqn (2) was fit to the experimental data shown in Fig. 8. As can be seen, the experimental data were fitted well by eqn (2). In the fitting process, the ΔE values were 758.3, 768.4, 742.5 and 698.0 cm^{-1} for 3, 9, 15 and 30 mol% Er^{3+} doped samples, respectively. They are in good agreement with the calculated value (762.27 cm^{-1}) derived from the measured DC luminescence spectra in Fig. 3. This fact means that eqn (2) can explain well the temperature dependence of the green emissions intensity ratio.

To assess the optical temperature sensing ability of the studied samples, it was crucial to determine the temperature sensing sensitivity, which is usually defined as the change in rate of R per unit temperature and can be expressed as follows:[28]

$$S(T) = dR(T)/dT = A\exp(-\Delta E/kT)(\Delta E/kT^2) \quad (3)$$

By taking the above-derived values of C and $\Delta E/k$ into eqn (3), the sensitivity function $S(T)$ versus T for the studied samples was
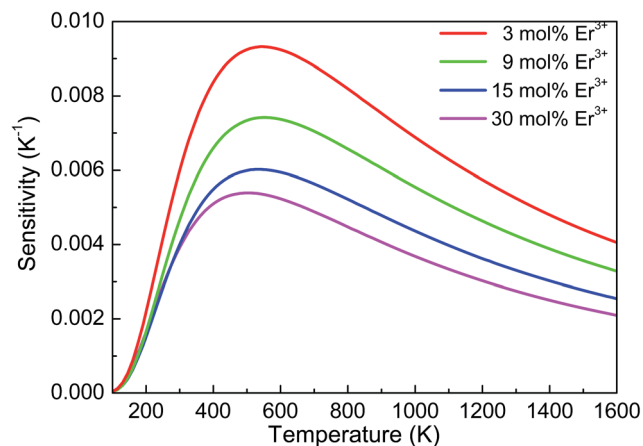
derived and are shown in Fig. 9 from 100–1600 K. It can be seen that the sensitivity curves of the four samples have the same change in trend. With an increase in temperature, the sensitivity first increases and reaches a maximum value and then slowly decreases with further increasing temperature. In addition, the sensitivity of the sample with lower Er^{3+} doping concentration was larger than that of high Er^{3+} concentration doping. When the Er^{3+} doping concentration was 3 mol%, the maximum sensitivity (S_{max}) reached 93×10^{-4} K^{-1} at 554 K. However, the maximum value of 30 mol% Er^{3+}-doped sample was only 54×10^{-4} K^{-1} at 509 K. A similar phenomenon was found in NaGdTiO$_4$:Er^{3+}/Yb^{3+} phosphors in our earlier study, which was ascribed to the different optical transition rate of Er^{3+} in various Er^{3+} doped samples based upon the results of absorption spectra.[20] Table 2 shows the comparison of the maximum sensitivity for Er^{3+} in some different host materials.[14,16,29–34] It can be seen that the sensitivity of Er^{3+} obtained in this study was a little higher than most of the sensitivities reported in other Er^{3+}-doped host materials, implying that YNbO$_4$:Er^{3+} phosphors may have potential applications as optical temperature sensors. Moreover, because YNbO$_4$:Er^{3+} phosphors have good thermal stability (the firing temperature was as high as 1300 °C, and its crystal structure can be stable at a such high temperature), it may be a good candidate for temperature sensing in high temperature environments.

4. Conclusions

In summary, the YNbO$_4$ phosphors with various Er^{3+} concentrations were successfully synthesized via a traditional high temperature solid-state reaction method. The crystal structure of the phosphors was identified by XRD, and single-phase YNbO$_4$ phosphors were obtained. The relative intensity of the green and the red emissions was significantly different in DC and UC luminescence processes, which can be ascribed to the different populated routes and pumped conditions. The quenching process of the green emissions from Er^{3+} in the DC luminescence process was well explained by the Van model, and the electric dipole–dipole interaction was confirmed to be responsible for the quenching behavior. According to the laser working current dependent UC luminescence spectra, it was

Fig. 9 Dependences of sensitivities on temperature of YNbO$_4$:x mol% Er^{3+} (x = 3, 9, 15, 30) samples.

confirmed that two and three photon absorption processes were involved in both of the green and red UC luminescence, respectively, irradiated by 980 and 1550 nm infrared wavelengths. Er^{3+} concentration dependent temperature sensing properties of $YNbO_4$:Er^{3+} samples were studied, and the temperature sensing curves were obtained by analyzing the temperature-dependent DC luminescence spectra. It was found that the sample with low Er^{3+} doping concentration had a high temperature sensitivity.

Acknowledgements

References

1 Z. Chen, X. W. Zhang, S. F. Zeng, Z. J. Liu, Z. J. Ma, G. P. Dong, S. F. Zhou, X. F. Liu and J. R. Qiu, *Appl. Phys. Express*, 2015, **8**, 032301–032305.

2 Y. Q. Qu, X. G. Kong, Y. J. Sun, Q. H. Zeng and H. Zhang, *J. Alloys Compd.*, 2009, **19**, 493–496.

3 F. Wang, Y. Han, C. S. Lim, Y. H. Lu, J. Wang, J. Xu, H. Y. Chen, C. Zhang, M. H. Hong and X. G. Liu, *Nature*, 2010, **463**, 1061–1065.

4 X. Y. Huang, S. Y. Han, W. Hu and X. G. Liu, *Chem. Soc. Rev.*, 2013, **42**, 173–201.

5 W. Yu, W. Xu, H. W. Song and S. Zhang, *Dalton Trans.*, 2014, **43**, 6139–6147.

6 W. Xu, Z. G. Zhang and W. W. Cao, *Opt. Lett.*, 2012, **37**, 4865–4867.

7 H. Zheng, S. Y. Xiang and B. J. Chen, *Chin. J. Lumin.*, 2014, **35**, 800–806.

8 D. Jaque and F. Vetrone, *Nanoscale*, 2012, **4**, 4301–4326.

9 S. F. León-Luis, U. R. Rodríguez-Mendoza, E. Lalla and V. Lavín, *Sens. Actuators, B*, 2011, **158**, 208–213.

10 T. Yue, B. N. Tian, C. Cui, P. Huang, L. Wang and B. J. Chen, *RSC Adv.*, 2015, **5**, 14123–14128.

11 R. Calderon-Villajos, C. Zaldo and C. Cascales, *Nanotechnology*, 2012, **23**, 3847–3856.

12 Y. Y. Zhou, Q. Ma, M. K. Lu, Z. F. Qiu and A. Y. Zhang, *J. Phys. Chem.*, 2008, **112**, 19901–19907.

13 A. Dwivedi, A. K. Sinqh and S. B. Rai, *Dalton Trans.*, 2014, **43**, 15906–15914.

14 Y. Y. Tian, Y. Tian, P. Huang, L. Wang, Q. F. Shi and C. Cui, *Chem. Eng. J.*, 2016, **297**, 26–34.

15 B. N. Tian, B. J. Chen, J. S. Sun, X. P. Li, J. S. Zhang and R. N. Hua, *Mater. Res. Express*, 2016, **3**, 116201.

16 A. K. Singh, S. K. Singh, B. K. Gupta, R. Prakash and S. B. Rai, *Dalton Trans.*, 2013, **42**, 1065.

17 H. Zhong, X. P. Li, R. S. Shen, J. S. Zhang, J. S. Sun, H. Y. Zhong, L. H. Cheng, Y. Tian and B. J. Chen, *J. Alloys Compd.*, 2012, **15**, 170–175.

18 A. C. Larson and R. B. Von Dreele, *Los Alamos National Laboratory Report LAUR*, 1994, pp. 86–748.

19 B. H. Toby, *J. Appl. Crystallogr.*, 2001, **34**, 210.

20 J. Bang, M. Abboudi, B. Abrams and P. H. Holloway, *J. Lumin.*, 2004, **106**, 177–185.

21 X. P. Li, X. Wang, H. Zhong, L. H. Cheng, S. Xu, J. S. Sun, J. S. Zhang, X. J. Li, L. L. Tong and B. J. Chen, *Ceram. Int.*, 2016, **42**, 14710–14715.

22 J. J. Li, J. S. Sun, J. T. Liu, X. P. Li, J. S. Zhang, Y. Tian, S. B. Fu, L. H. Cheng, H. Y. Zhong, H. P. Xia and B. J. Chen, *Mater. Res. Bull.*, 2013, **48**, 2159–2165.

23 U. Van, *J. Electrochem. Soc.*, 1967, **114**, 1048–1053.

24 H. M. Noh, H. K. Yang, B. K. Moon, B. C. Choi, J. H. Jeong, H. Choi and J. H. Kim, *J. Appl. Phys.*, 2013, **52**, 765–773.

25 K. Annapoorani, N. S. Murthy, T. R. Ravindran and K. Marimuthu, *J. Lumin.*, 2016, **171**, 19–26.

26 Y. Fu, Y. Shi, N. Zhang, Y. Tian, M. M. Xing and X. X. Luo, *Mater. Res. Bull.*, 2016, **84**, 346–349.

27 Y. Shen, X. Wang, H. C. He, Y. H. Lin and C. W. Nan, *Sci. Technol.*, 2012, **5**, 1008–1011.

28 G. Tripathi, V. K. Rai and S. B. Rai, *Opt. Mater.*, 2007, **8**, 201–206.

29 P. V. dos Santos, M. T. de Araujo, A. S. Gouveria-Neto, J. A. Medeiros Neto and A. S. B. Sombra, *IEEE J. Quantum Electron.*, 1999, **35**, 395–399.

30 X. Wang, X. G. Kong, Y. Yu, Y. J. Sun and H. Zhang, *J. Phys. Chem. C*, 2007, **111**, 15119–15124.

31 S. F. León-Luis, U. R. Rodríguez-Mendoza, E. Lalla and V. Lavín, *Sens. Actuators, B*, 2011, **11**, 208–213.

32 C. R. Li, B. Dong, C. G. Ming and M. K. Lei, *Sensors*, 2007, **7**, 2652–2659.

33 A. Camargo, J. F. Possatto, L. Nunes, E. R. Botero, E. R. M. Andreeta, D. Garcia and J. A. Eiras, *Solid State Commun.*, 2006, **137**, 1–5.

34 Z. P. Cai, H. Y. Xu, P. Feron, M. Mortier and G. Stephan, *Sens. Actuators, A*, 2003, **65**, 187–192.